Inverted Dirac-electron population for broadband lasing in a thermally activated *p*-type topological insulator

K. Sumida,^{1,*} Y. Ishida,^{2,†} T. Yoshikawa,¹ J. Chen,¹ M. Nurmamat,¹ K. A. Kokh,^{3,4,5} O. E. Tereshchenko,^{4,5,6} S. Shin,² and A. Kimura^{1,‡}

¹Graduate School of Science, Hiroshima University, 1-3-1 Kagamiyama, Higashi-Hiroshima 739-8526, Japan

²ISSP, University of Tokyo, 5-1-5 Kashiwa-no-ha, Kashiwa, Chiba 277-8581, Japan

³Institute of Geology and Mineralogy, Siberian Branch, Russian Academy of Sciences, Koptyuga pr. 3, 630090 Novosibirsk, Russia

⁴Physics Department, Novosibirsk State University, ul. Pirogova 2, 630090 Novosibirsk, Russia

⁵Physics Department, Saint Petersburg State University, Saint Petersburg, 198504, Russia

⁶Institute of Semiconductor Physics, Siberian Branch, Russian Academy of Sciences,

pr. Akademika Lavrent'eva 13, 630090 Novosibirsk, Russia

(Received 25 December 2017; revised manuscript received 11 June 2018; published 1 February 2019)

Maintaining a population inversion in electron distributions is the first step towards lasing. There is a strong interest in realizing the inversion in a Dirac conical band structure, because broad-band lasing may then be realized owing to the zero-gap nature of the Dirac cone. Here we show that the population inversion can be elongated to >7 ps at 8 K and >10 ps at 300 K on the surface of a p-type topological insulator (Sb_{0.73}Bi_{0.27})₂Te₃. Time- and angle-resolved photoemission spectroscopy gives us the direct evidence for the elongated duration of the inversion in the topological surface states. We hereby provide a guideline to prolong the population inversion at finite temperatures. Our study strengthens the route toward the Dirac materials to be a lasing medium.

DOI: 10.1103/PhysRevB.99.085302

I. INTRODUCTION

Dirac materials possess Dirac fermions characterized by the zero-gap and conical band dispersions. Dirac fermions are realized in graphitic materials [1], on the surface of topological insulators (TIs) [2,3], and in three-dimensional (3D) Dirac semimetals such as Cd₃As₂ [4-6]. Dirac materials have the potential to revolutionize lasers [7]: If a population inversion can be maintained across the Dirac point of the conical band structure, induced emission can occur for whatever color, even in the THz region [8] (Fig. 1, lower right schematic). Wide-band mode locking is already demonstrated in a variety of Dirac materials [9,10], indicating that the optical filling of the upper Dirac cone is substantial when the optical pumping is intense enough. The surface of TIs may be used as an optical gain medium for broad-band lasing if the duration of an inverted population in the topological surface states (TSSs) can be elongated.

Time- and angle-resolved photoemission spectroscopy (TARPES) is a pump-and-probe method and can visualize the electron distributions after the optical pump in a time-, energy-, and momentum-resolved manner. Being a surface sensitive method, TARPES is the suited method to verify the population inversions occurring on TIs. The first evidence for the population inversion in the TSS was found in a naturally hole-doped (p-type) TI, Sb₂Te₃ [11]. However, the duration of the inversion was \sim 3 ps at most. Even though the \sim 3-ps

duration is longer than the nonthermal and possibly inverted distributions reported for graphitic materials [12–14], further elongation would be the requisite for the ultimate goal of broad-band lasing. In addition, from the application point of view, the demonstration is better done at room temperature, where thermally-activated electrons also exist and may affect the duration.

In this paper, we investigate the carrier dynamics of a p-type TI (Sb_{0.73}Bi_{0.27})₂Te₃ by using TARPES. Our main focus is in the investigation into how the dynamics is affected by the thermally-excited carriers. We show that the duration of the nonequilibrated state is prolonged at elevated temperatures, where the thermally-excited electrons coexist and partially fill up to the Dirac point. Furthermore, the duration of the population inversion across the Dirac point is also prolonged from >7 ps at 8 K to >10 ps at 300 K. We attribute the elongation to the thermally enhanced blocking near the Dirac point at 300 K. Our finding shows the ability to control the degree of population inversion and provides a guideline towards the realization of broad-band lasing using TIs at practical temperature.

II. EXPERIMENTAL

High quality $(Sb_{0.73}Bi_{0.27})_2Te_3$ single crystal was grown by the Bridgman method [15]. Atomic ratios of the constituent elements were determined by using electron probe micro analysis. TARPES spectrometer consisted of a hemispherical electron analyzer and a Ti:sapphire laser system that delivered 1.48-eV pump and 5.92-eV probe pulses at the repetition rate of 250 kHz [16]. The pump and probe pulses had spot diameters of 280 and 85 μ m, respectively, on the sample.

^{*}sumida1126@hiroshima-u.ac.jp

[†]ishiday@issp.u-tokyo.ac.jp

[‡]akiok@hiroshima-u.ac.jp

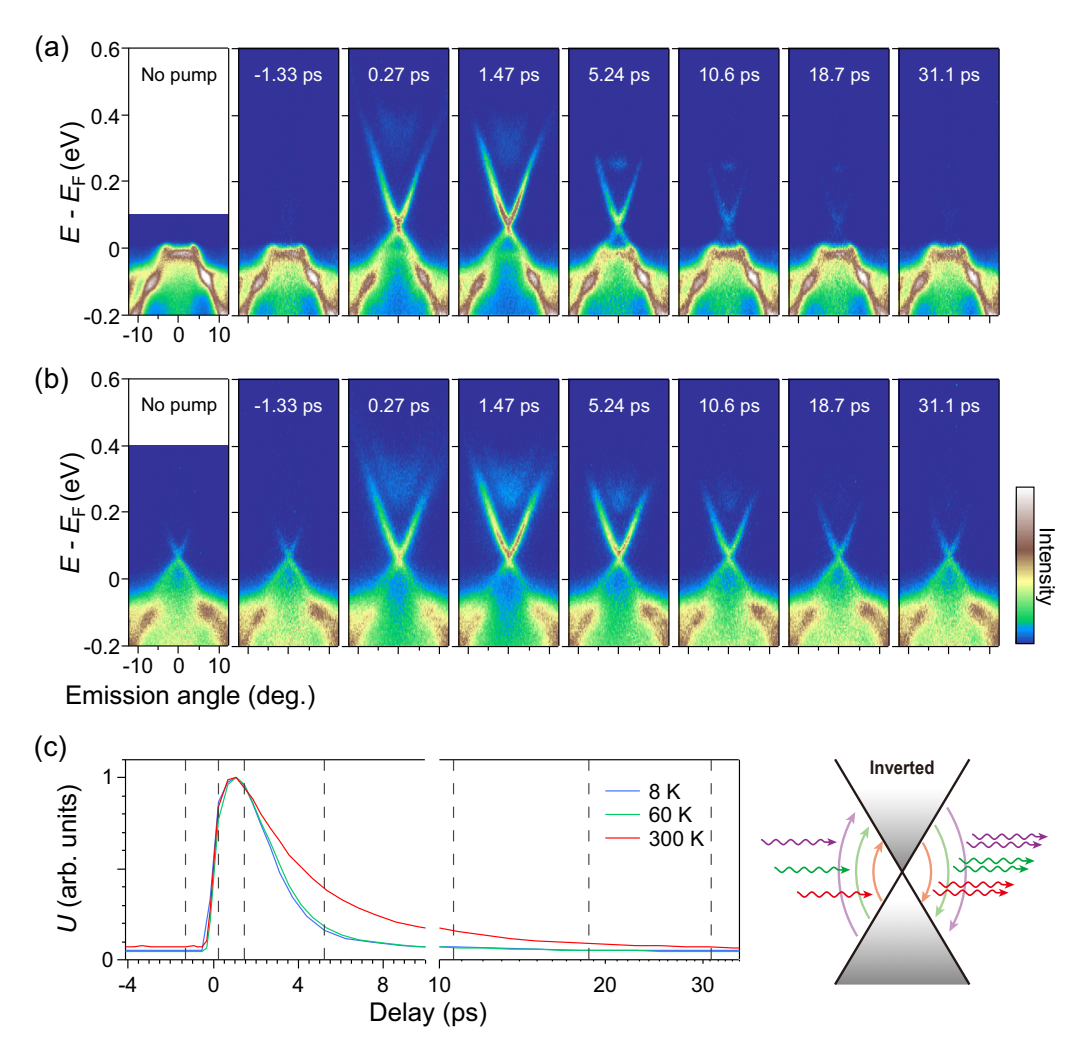


FIG. 1. Temperature-dependent photoexcited carrier dynamics in the $(Sb_{0.73}Bi_{0.27})_2Te_3$ crystal. TARPES images recorded at various pump-probe delay times at 8 K (a) and 300 K (b). The all cuts are along the $\overline{\Gamma}$ - \overline{K} direction. (c) Time- and temperature-dependent electronic energy U estimated at T=8, 60, and 300 K (see text for more details). Dashed lines indicate the delay times of TARPES images shown in panels (a) and (b). Schematic of population inversion and broad-band lasing in Dirac material (right).

The energy and time resolutions were 15 meV and 300 fs, respectively. The TARPES measurements were carried out at the pumping fluence of 0.13 mJ/cm². Samples were cleaved in the spectrometer at the base pressure 1×10^{-8} Pa. Spectral broadenings due to space charge effects were set to $\lesssim 10$ meV.

III. RESULTS AND DISCUSSION

First, we show the band dispersions and carrier dynamics recorded at low temperature. Figure 1(a) shows the TARPES images recorded at various pump-probe delay times (t) at T=8 K. All the images show the dispersions along the $\overline{\Gamma}$ - \overline{K} line. In the leftmost column, the image recorded without pumping is also displayed. Before the arrival of the pump pulse (t=-1.33 ps), the photoemission intensity is observed only below $E_{\rm F}$, in which no recognizable difference appears compared with that recorded without pumping. This shows that surface photovoltage effects are absent in the present sample [17,18]. After the arrival of the pump pulse, the electrons are immediately populated in the TSS and the bulk conduction bands located above $E_{\rm F}$. Then, the entire Dirac-

cone-like TSS is visualized, for instance at t = 0.27, 1.47, and 5.24 ps due to the transient population. During the recovery, the photoexcited electrons are transferred to lower energy by scatterings [19,20] but some electrons remained at the bottom of the bulk conduction band; see the image at 5.24 ps. At 10 ps, the relaxation in the LDC is mostly accomplished. However, the photoexcited carriers are still remaining in the UDC; that is, an inverted population across the Dirac point is realized. Such an inverted population was also observed in a pure Sb₂Te₃, although the duration of the inverted population was at most ~ 3 ps [11]. The electronic recovery time of the present sample is slightly longer than that of Sb₂Te₃ [11] but much shorter than that of $(Sb_{0.57}Bi_{0.43})_2Te_3$ which has a higher Bi concentration than the present specimen [21]. The elongation of the recovery upon the increase of the Bi content was attributed to the approach of the Dirac point towards $E_{\rm F}$ due to the conical shape of the TSS: The available phase space for the scattering within the Dirac cone (intraband scattering) becomes small when $E_{\rm F}$ approaches the Dirac point [21].

Next, we look into the carrier dynamics recorded at 300 K, see Fig. 1(b). TARPES images recorded at t = -1.33 ps are

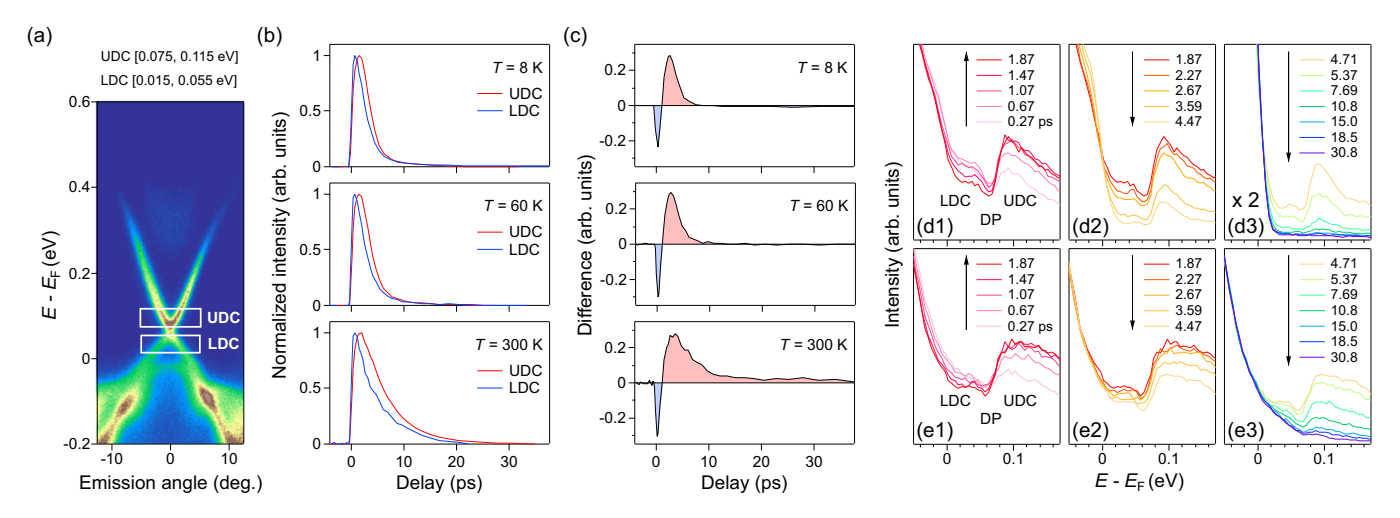


FIG. 2. (a) TARPES image of $(Sb_{0.73}Bi_{0.27})_2Te_3$ along the $\overline{\Gamma}$ - \overline{K} line recorded at t=1.33 ps. Energy-angle frames are set at the upper and lower Dirac cones (UDC and LDC) in the angular range of ± 5 degrees and in the energy ranges of [0.077, 0.115 eV] and [0.015, 0.055 eV], respectively. (b) Temperature-dependent photoemission intensities integrated within the frames UDC and LDC are plotted as a function of the pump-probe delay time recorded at T=8 (upper), 60 (middle), and 300 K (lower), respectively. (c) Difference of photoemission intensity (UDC – LDC). Red regions denote the intensity deference in a time domain where the inverted population takes place. Angle-integrated EDCs recorded at T=8 (d1)–(d3) and 300 K (e1)–(e3) in the time regions of $0.27 \le t \le 1.87$ ps, $1.87 \le t \le 4.47$ ps, and $4.47 \le t \le 30.8$ ps.

unchanged from the equilibrium state recorded without pumping, as in the case at 8 K. However, there are the following differences between 8 and 300 K. First, the electronic recovery time is prolonged to >30 ps. Second, even before the arrival of the pump pulse, the lower part of the Dirac cone is already filled due to the thermal broadening at 300 K.

In order to quantify the temperature-induced modifications in the carrier dynamics, we estimate the following integral $U(t) \equiv \int_{\omega>0} \omega I(\omega,t) d\omega$, which represents the electronic energy retained by the electrons above $E_{\rm F}$. Here, $\omega=E-E_{\rm F}$, and $I(\omega,t)$ is the angle-integrated photoemission intensity. In Fig. 1(c), we plot U(t) of T=8, 60, and 300 K. Upon the arrival of the pump pulse, U(t) sharply rises around 0 ps and peaks at \sim 1 ps for all temperatures. The pump-induced changes at 300 K remain even at >30 ps while those at 8 and 60 K are almost recovered within \sim 10 ps.

Next, in order to see the energy-dependent carrier dynamics in the surface state at each temperature, we set the frames at the upper and lower parts of the Dirac cone (UDC and LDC) across the Dirac point as shown in Fig. 2(a) and plot the normalized photoemission intensity as a function of the pumpprobe delay time in Fig. 2(b). In the LDC region, we observed a fast rise of intensity at all temperatures. Subsequently, the intensities at UDC are maximized with some delays. The most striking feature is that even though the energy of UDC is higher than that of LDC, the electronic recovery at UDC is longer than that at LDC. This indicates that the transient inverted Dirac electron population is realized. To show the duration of the inverted population more clearly, we plot the photoemission intensity difference between UDC and LDC in Fig. 2(c). At T = 8 and 60 K (upper and middle panels), the population inversion appears in the time domain from \sim 1 ps to \sim 7 ps. The difference between two temperatures is negligibly small. At 300 K, the duration of the inverted population (lower panel) is much longer than those observed at lower temperatures. The duration is prolonged to >10 ps even though this sample is not an intrinsic (bulk-insulating) TI.

To provide further evidence for the prolonged population inversion, we show in Figs. 2(d) and 2(e) the transient angle-integrated energy distribution curves (EDCs) recorded at T=8 and 300 K, respectively. In both cases, from 0.67 to 1.87 ps, the increased spectral intensities in the UDC region are higher than those in the LDC region [Figs. 2(d1) and 2(e1)]. The results clearly show that the population inversion is taking place. After the spectral intensities reached maximum at \sim 1.5 ps in the UDC region, they become smaller with the population inversion being maintained [Figs. 2(d2) and 2(e2)]. At T=300 K, the population inversion is retained for >10 ps in contrast to the case at 8 K [Figs. 2(d3) and 2(e3)]. These results are in good agreement with the observation from the data shown in Figs. 2(b) and 2(c).

Here, we consider the instantaneous and delayed rises in the LDC across the $E_{\rm F}$ and UDC observed in Fig. 2(b), respectively. An instantaneous rise is often observed in the vicinity of $E_{\rm F}$ in metallic materials [11,21–23]. In the present

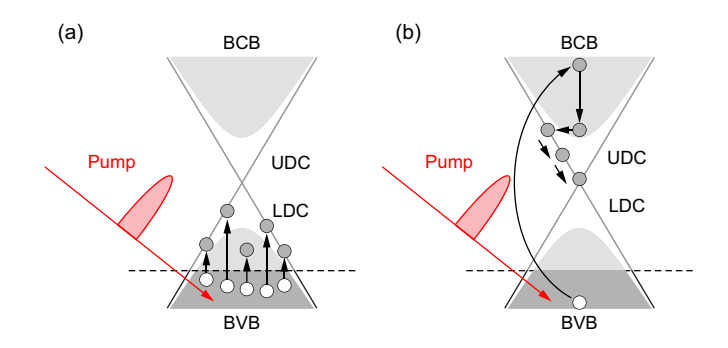


FIG. 3. Schematics of two different filling mechanisms at UDC and LDC. (a) Impact-ionization-like process in the vicinity of $E_{\rm F}$. (b) Indirect transition process by intraband and interband scatterings.

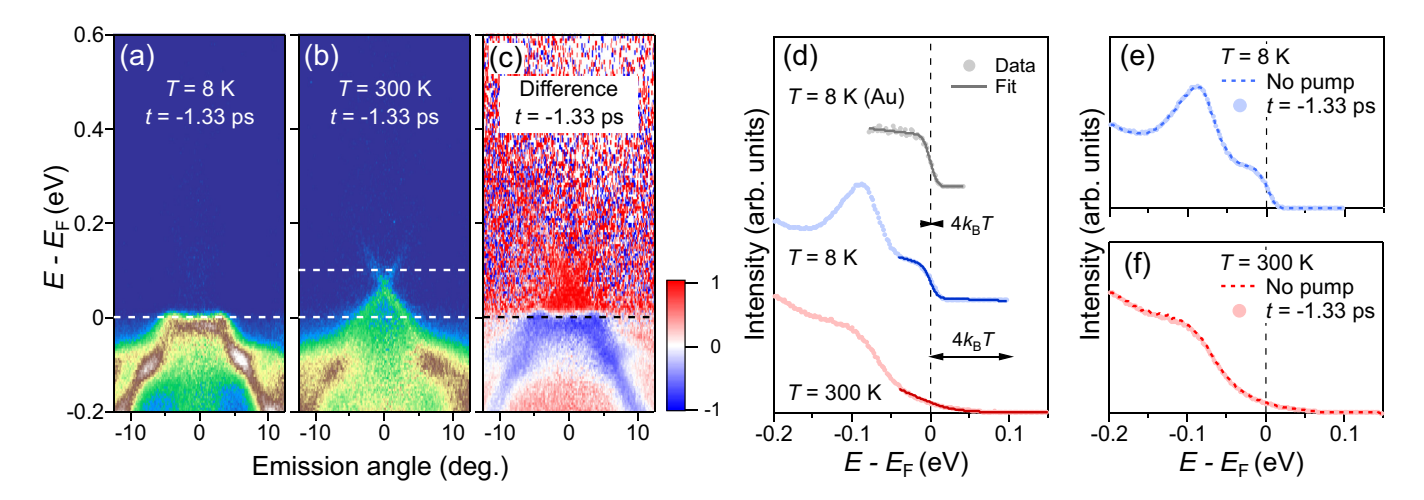


FIG. 4. Thermal-induced modulation of TARPES images. (a),(b) TARPES images recorded at T=8 and 300 K in equilibrium state (t=-1.33 ps). (c) Difference image between the images acquired at T=8 and 300 K. (d) Angle-integrated EDCs of the images shown in (a) and (b) fitted by the Fermi-Dirac distribution function. The energy scale of $4k_BT$ at each temperature and the Fermi edge of Au at 8 K are also shown in (d). (e),(f) Angle-integrated EDCs recorded without and with pumping at t=-1.33 ps at 8 (e) and 300 K (f).

case, the $E_{\rm F}$ is located in the LDC and bulk valence band, and the instantaneous rise therein may have a common origin to those observed in metals. A mechanism is similar to the impact ionization, which can explain the instantaneous rise around the $E_{\rm F}$ in metallic materials [Fig. 3(a)]. It probably dominates the filling at the LDC and its duration is relatively fast. On the other hand, the delayed rise seen in the UDC is mainly due to an indirect transition process by intraband and interband scatterings depicted in Fig. 3(b). It can cause some delayed responses at the UDC comparing at the LDC because the UDC is filled after the transfer of the excited electrons from the bulk conduction band.

Although TIs are characterized by the spin-momentum locking nature on their surfaces, that is not pure spin-momentum locking [24–27]. That is, there are multiple orbital components that contribute in forming a particular TSS. As a result, both up and down spin components also coexist in the particular state. Therefore, the direct transition between UDC and LDC and hence the lasing operation within the Dirac mode on TI surface becomes allowed.

We turn our attention to the thermally activated electrons observed at T = 300 K. Figures 4(a) and 4(b) display the equilibrated TARPES images recorded at t =-1.33 ps. Figure 4(c) shows the difference between the two TARPES images shown in Figs. 4(a) and 4(b). At T = 8 K, the photoemission intensity is observed only below $E_{\rm F}$. However, at T=300 K, some part of LDC is already occupied even before the arrival of the pump pulse, and the maximum energy of the electron occupation is shifted towards higher energy by ~ 100 meV. Figure 4(d) shows angle-integrated EDCs of the images presented in Figs. 4(a) and 4(b) fitted by the Fermi-Dirac distribution function. The energy scale of $4k_BT$ at each temperature and the Fermi edge of Au recorded at reduced probing power at 8 K are also shown in Fig. 4(d). All EDCs are well reproduced by the fitting. Comparing the spectrum of Au with that of the present sample at 8 K, we can confirm that the space charge effect is less efficient. Moreover, Figs. 4(e) and 4(f) show the EDCs recorded without and with pumping at t=-1.33 ps at 8 and 300 K. The difference between two EDCs is also negligibly small. Thus, we can exclude a possibility of the surface photovoltage effect reported so far in the bulk insulating regime [17,18,21]. Concerning the temperature dependence of the chemical potential shift, we can confirm that there is a small shift of the locus of the Dirac point by comparing Figs. 2(d) and 2(e). However, this shift is less than 10 meV and too small to explain why the spectral weight tailing into the unoccupied side \sim 100 meV at 300 K. Therefore, the tailing of the EDC into the unoccupied side is mainly attributed to the thermal broadening at 300 K: The tailing of 100 meV is comparable $4k_{\rm B}T$ at 300 K.

The Dirac point of the present sample is located at \sim 100 meV above the $E_{\rm F}$, which coincidences to the energy scale of the thermal broadening of the Fermi-Dirac distribution function around the $E_{\rm F}$. This implies that, if the Dirac point is located at \sim 4 $k_{\rm B}T$ above the $E_{\rm F}$, there is a high chance to have a strongly-inverted population when the sample temperature is held at T. This can be the new guideline towards realizing the "Dirac laser" at practical temperatures [7].

Finally, we discuss the origin of the prolonged duration of the inverted population. At low temperature, since the density of states around the Dirac node is close to zero, the available phase space is probably restricted. This can prevent the photoexcited electrons from recombining with holes as depicted in Fig. 5 (left), so that the electrons pile up just above the Dirac node. As a result, the population inversion takes place across the Dirac point [11]. At high temperature, the electrons are thermally excited and partially fill the states up to the Dirac node above $E_{\rm F}$. This certainly promotes more substantial Pauli blocking and prolongs the recovery time as schematically shown in Fig. 5 (right).

Note that the prolonged duration of nonequilibrated state, which exceeded >400 ps, was recently reported in neutral topological insulator $(Sb_{0.57}Bi_{0.43})_2Te_3$ [21]. However, we were not able to discern the population inversion therein: The lower part of the Dirac cone appeared to be almost fully

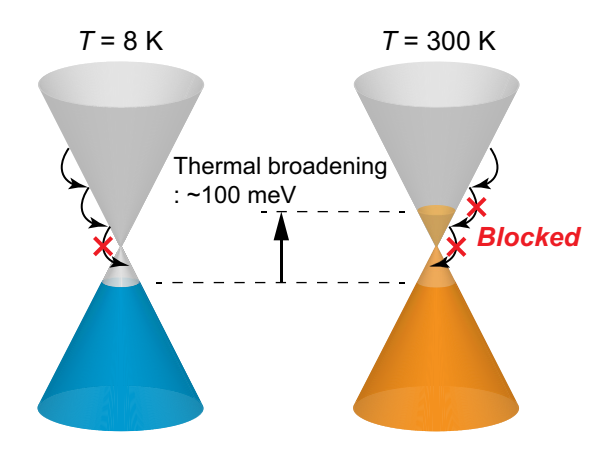


FIG. 5. Schematics of relaxation process of photoexcited electrons in the surface Dirac cones at low (left) and high (right) temperatures.

occupied. Even when the pumping fluence was increased to 0.52 mJ/cm², which is four times larger than the present case, the signatures of the population inversion were not observed.

IV. CONCLUSION

In conclusion, the present TARPES study of the p-type $(Sb_{0.73}Bi_{0.23})_2Te_3$ demonstrates that the duration of the inverted Dirac fermion population can be prolonged to >10 ps at room temperature. Because of the elongation, p-type TIs would be suited for a broad-band lasing medium operable at room temperature.

ACKNOWLEDGMENTS

This work was carried out by the joint research in the Institute for Solid State Physics, the University of Tokyo. This work was partly supported by the bilateral collaboration program between RFBR (Russia, Grant No. 15-52-50017) and JSPS (Japan) and also by KAKENHI Grants No. 26800165, No. 17H06138, No. 18H01148, and No. 18H03683. K.S. was financially supported by a Grant-in-Aid for JSPS Fellows (Grant No. 16J03874). The study has also been supported by the Russian Science Foundation (Grant No. 17-12-01047) and RFBR (Grant No. 17-08-00955) in part of the single crystal growth and samples characterization.

- [1] A. K. Geim and K. S. Novoselov, The rise of Graphene, Nat. Mater. 6, 183 (2007).
- [2] M. Z. Hasan and C. L. Kane, Colloquium: Topological insulators, Rev. Mod. Phys. **82**, 3045 (2010).
- [3] X. L. Qi and S. C. Zhang, Topological insulators and superconductors, Rev. Mod. Phys. **83**, 1057 (2011).
- [4] Z. K. Liu, J. Jiang, B. Zhou, Z. J. Wang, Y. Zhang, H. M. Weng, D. Prabhakaran, S-K. Mo, H. Peng, P. Dudin, T. Kim, M. Hoesch, Z. Fang, X. Dai, Z. X. Shen, D. L. Feng, Z. Hussain, and Y. L. Chen, A stable three-dimensional topological Dirac semimetal Cd₃As₂, Nat. Mater. 13, 677 (2014).
- [5] M. Neupane, S.-Y. Xu, R. Sankar, N. Alidoust, G. Bian, C. Liu, I. Belopolski, T.-R. Chang, H.-T. Jeng, H. Lin, A. Bansil, F. Chou, and M. Z. Hasan, Observation of a three-dimensional topological Dirac semimetal phase in high-mobility Cd₃As₂, Nat. Commun. 5, 3786 (2014).
- [6] S. Borisenko, Q. Gibson, D. Evtushinsky, V. Zabolotnyy, B. Büchner, and R. J. Cava, Experimental Realization of a Three-Dimensional Dirac Semimetal, Phys. Rev. Lett. 113, 027603 (2014).
- [7] F. Bonaccorso, Z. Sun, T. Hasan, and A. C. Ferrari, Graphene photonics and optoelectronics, Nat. Photonics 4, 611 (2010).
- [8] T. Otsuji, S. A. Boubanga Tombet, A. Satou, H. Fukidome, M. Suemitsu, E. Sano, V. Popov, M. Ryzhii, and V. Ryzhii, Graphene-based devices in terahertz science and technology, J. Phys. D: Appl. Phys. 45, 303001 (2012).
- [9] Q. Bao and K. P. Loh, Graphene Photonics, Plasmonics, and Broadband Optoelectronics Devices, ACS Nano 6, 3677 (2012).
- [10] F. Bonaccorso and Z. Sun, Solution processing of graphene, topological insulators and other 2d crystals for ultrafast photonics, Opt. Mater. Exp. 4, 63 (2014).
- [11] S. Zhu, Y. Ishida, K. Kuroda, K. Sumida, M. Ye, J. Wang, H. Pan, M. Taniguchi, S. Qiao, S. Shin, and A. Kimura, Ultrafast electron dynamics at the Dirac node of the topological insulator Sb₂Te₃, Sci. Rep. 5, 13213 (2015).

- [12] Y. Ishida, T. Togashi, K. Yamamoto, M. Tanaka, T. Taniuchi, T. Kiss, M. Nakajima, T. Suemoto, and S. Shin, Non-thermal hot electrons ultrafastly generating hot optical phonons in graphite, Sci. Rep. 1, 64 (2011).
- [13] I. Gierz, M. Mitrano, J. C. Petersen, C. Cacho, I. C. E. Turcu, E. Springate, A. Stöhr, A. Köhler, U. Starke, and A. Cavalleri, Population inversion in monolayer and bilayer graphene, J. Phys.: Condens. Matter 27, 164204 (2015).
- [14] A. Stange, C. Sohrt, L. X. Yang, G. Rohde, K. Janssen, P. Hein, L.-P. Oloff, K. Hanff, K. Rossnagel, and M. Bauer, Hot electron cooling in graphite: Supercollision versus hot phonon decay, Phys. Rev. B 92, 184303 (2015).
- [15] K. A. Kokh, S. V. Makarenko, V. A. Golyashov, O. A. Shegai, and O. E. Tereshchenko, Melt growth of bulk Bi₂Te₃ crystals with a natural *p-n* junction, CrystEngComm 16, 581 (2014).
- [16] Y. Ishida, T. Togashi, K. Yamamoto, M. Tanaka, T. Kiss, T. Otsu, Y. Kobayashi, and S. Shin, Time-resolved photoemission apparatus achieving sub-20-meV energy resolution and high stability, Rev. Sci. Instrum. 85, 123904 (2014).
- [17] Y. Ishida, T. Otsu, T. Shimada, M. Okawa, Y. Kobayashi, F. Iga, T. Takabatake, and S. Shin, Emergent photovoltage on SmB₆ surface upon bulk-gap evolution revealed by pump-and-probe photoemission spectroscopy, Sci. Rep. 5, 8160 (2015).
- [18] M. Neupane, S.-Y. Xu, Y. Ishida, S. Jia, B. M. Fregoso, C. Liu, I. Belopolski, G. Bian, N. Alidoust, T. Durakiewicz, V. Galitski, S. Shin, R. J. Cava, and M. Z. Hasan, Gigantic Surface Life-Time of an Intrinsic Topological Insulator, Phys. Rev. Lett. 115, 116801 (2015).
- [19] S.-L. Yang, J. A. Sobota, D. Leuenberger, Y. He, M. Hashimoto, D. H. Lu, H. Eisaki, P. S. Kirchmann, and Z.-X. Shen, Inequivalence of Single-Particle and Population Lifetimes in a Cuprate Superconductor, Phys. Rev. Lett. 114, 247001 (2015).
- [20] J. D. Rameau, S. Freutel, A. F. Kemper, M. A. Sentef, J. K. Freericks, I. Avigo, M. Ligges, L. Rettig, Y. Yoshida, H. Eisaki,

- J. Schneeloch, R. D. Zhong, Z. J. Xu, G. D. Gu, P. D. Johnson, and U. Bovensiepen, Energy dissipation from a correlated system driven out of equilibrium, Nat. Commun. 7, 13761 (2016).
- [21] K. Sumida, Y. Ishida, S. Zhu, M. Ye, A. Pertsova, C. Triola, K. A. Kokh, O. E. Tereshchenko, A. V. Balatsky, S. Shin, and A. Kimura, Prolonged duration of nonequilibrated Dirac fermions in neutral topological insulators, Sci. Rep. 7, 14080 (2017).
- [22] M. Neupane, Y. Ishida, R. Sankar, J.-X. Zhu, D. S. Sanchez, I. Belopolski, S.-Y. Xu, N. Alidoust, M. M. Hosen, S. Shin, F. Chou, M. Z. Hasan, and T. Duraliewicz, Electronic structure and relaxation dynamics in a superconducting topological material, Sci. Rep. 6, 22557 (2016).
- [23] Y. Ishida, H. Masuda, H. Sakai, S. Ishiwata, and S. Shin, Revealing the ultrafast light-to-matter energy conversion before heat diffusion in a layered Dirac semimetal, Phys. Rev. B 93, 100302(R) (2016).

- [24] S. R. Park, J. Han, C. Kim, Y. Y. Koh, C. Kim, H. Lee, H. J. Choi, J. H. Han, K. D. Lee, N. J. Hur, M. Arita, K. Shimada, H. Namatame, and M. Taniguchi, Chiral Orbital-Angular Momentum in the Surface States of Bi₂Se₃, Phys. Rev. Lett. 108, 046805 (2012).
- [25] Z.-H. Zhu, C. N. Veenstra, G. Levy, A. Ubaldini, P. Syers, N. P. Butch, J. Paglione, M. W. Haverkort, I. S. Elfimov, and A. Damascelli, Layer-By-Layer Entangled Spin-Orbital Texture of the Topological Surface State in Bi₂Se₃, Phys. Rev. Lett. 110, 216401 (2013).
- [26] Y. Cao, J. A. Waugh, X.-W. Zhang, J.-W. Luo, Q. Wang, T. J. Reber, S. K. Mo, Z. Xu, A. Yang, J. Schneeloch, G. D. Gu, M. Brahlek, N. Bansal, S. Oh, A. Zunger, and D. S. Dessau, Mapping the orbital wavefunction of the surface states in three-dimensional topological insulators, Nat. Phys. 9, 499 (2013).
- [27] H. Zhang, C.-X. Liu, and S.-C. Zhang, Spin-Orbital Texture in Topological Insulators, Phys. Rev. Lett. 111, 066801 (2013).